

A method to infer the stellar population that dominated the UV background at the end of reionization

Michael R. Santos¹ * and Abraham Loeb^{2,3}

¹*Theoretical Astrophysics, 130-33 Caltech, Pasadena, CA 91125, USA*

²*Astronomy Department, Harvard University, 60 Garden St., Cambridge, MA 02138, USA*

³*Guggenheim fellow; currently on sabbatical leave at the Institute for Advanced Study, Princeton, NJ 08540, USA*

2 November 2018

ABSTRACT

We present an observational test of the spectrum of the ionizing background at $z \simeq 5$; the test is sufficiently sensitive to determine whether Pop II or Pop III stars are the dominant source of ionizing radiation. The ionizing background at $z \simeq 5$ may reflect the nature of the sources responsible for the final overlap phase of reionization. We find that rest-frame extreme-UV He I absorption will be detectable in deep spectral observations of some rare $z \simeq 5$ quasars; the ratio of He I to H I absorption reflects the shape of the ionizing background in the photon energy range between 13.6 and 24.6 eV. Most $z \simeq 5$ quasars have too much H I absorption along their line of sight for He I absorption to be observed. However, based on current measurements of H I absorber statistics, we use Monte Carlo simulations to demonstrate that the Sloan Digital Sky Survey (SDSS) will discover a sufficient number of $z \simeq 5$ quasars to turn up a quasar suitable for measuring He I absorption (and we illustrate a selection method to identify that quasar). From simulated observations of a suitable $z \simeq 5$ quasar with a 10-meter telescope, we show that a constraint on the spectral slope of the ionizing background at that redshift can be obtained.

Key words: quasars: absorption lines – intergalactic medium – diffuse radiation – cosmology: theory

1 INTRODUCTION

Intergalactic hydrogen is almost completely ionized by $z \simeq 6$ (Becker et al. 2001; Djorgovski et al. 2001), but the sources responsible for reionization are still not known (see Barkana & Loeb 2001 and Loeb & Barkana 2001 for reviews of the theoretical possibilities). A low neutral-hydrogen fraction is found at lower redshift even in relatively over-dense systems, despite the short (compared to the Hubble time) recombination time-scale in those systems. This implies a continued supply of ionizing photons after reionization completed. Measurements of the intensity of the ionizing background below $z \sim 3$ (Scott et al. 2000) are consistent with an ionizing background produced by observed quasars (Haardt & Madau 1996). At higher redshifts, however, the declining abundance of bright quasars (e.g., Fan et al. 2001b) suggests that they cannot provide an ionizing background sufficient to reionize the universe (Wyithe & Loeb 2003a), and this conclusion is supported by deep x-ray surveys (Barger et al. 2003).

Recent results from the *WMAP* satellite imply that reionization was substantially underway by $z \sim 15$ (Kogut et al. 2003; Spergel et al. 2003). However, quasar absorption studies at $z \simeq 6$ (Becker et al. 2001; Djorgovski et al. 2001) suggest a dramatic evolution in the ionizing background around that redshift. Some authors have reconciled the *WMAP* evidence for early reionization with the quasar result that reionization is just finishing at $z \simeq 6$ by postulating two reionizations of the universe (Cen 2003a,b; Wyithe & Loeb 2003a,b), generally invoking a hard Pop III stellar spectrum for the early reionization and a Pop II stellar spectrum for the final reionization at $z \simeq 6$.

The most direct technique to ascertain the sources responsible for the ionizing background at high redshift is to take a census of all sources that contribute ionizing photons. The advantage of this technique is that the relative contribution of different types of sources are measured directly, as are the spatial distributions and other properties of the populations. Unfortunately, the large luminosity distance to high redshift means that only the most luminous sources can be detected with current observational methods. For example, Fan et al. (2001b) measure a power-law high-redshift quasar luminosity function with a steep slope, but estimate

* E-mail: mrs@tapir.caltech.edu (MRS); loeb@cfa.harvard.edu (AL)

that the traditional power-law break of the quasar luminosity function would occur more than one magnitude below their survey limit: there is little constraint on the faint end of the quasar luminosity function from direct source detection.

A complementary method to direct detection is measurement of the properties of the integrated ionizing background. Although this technique does not identify ionizing sources directly, it is effective at detecting ionization due to a very abundant population of low-luminosity sources. Moreover, the shape of the integrated ionizing background is dictated by the combination of sources responsible for it; different spectra arise from various possible contributors, such as quasars (Telfer et al. 2002), Pop II OB stars (e.g., Leitherer et al. 1999), very massive metal-free (Pop III) stars (Bromm, Kudritzki & Loeb 2001), and x-rays from early stars (Oh 2001).

This paper describes possible observations that would constrain the spectral shape of the ionizing background just after reionization finished. In Section 2, we introduce quasar absorption line spectroscopy in the context of this paper. Section 3 describes our parametrization of the ionizing background, and the resulting ionization state of absorption systems in the intergalactic medium (IGM). In Section 4 we apply those results to observed statistics of H I absorbers to generate a model for H I and He I opacity toward high-redshift quasars; the assumed properties of the quasars are given in Section 5. The method of simulating line of sight (LOS) absorption spectra and studying the sensitivity of the results to the shape of the ionizing-background spectrum is described in Section 6. Section 7 presents a method to select the best quasars for absorption line spectroscopy. We summarize our results in Section 8.

2 ABSORPTION SPECTROSCOPY

The easiest way to make a crude measurement of the shape of the ionizing background is through the ionization state of photoionized IGM gas; in the next Section we show explicitly how the background spectrum is related to the ionization state. Atoms and ions with at least one bound electron in the ground state have strong bound-bound transition cross-sections, typically located at UV or soft x-ray energies. Consequently, even small amounts of these species on the line of sight to a background source produce strong absorption features. The most common extragalactic application of this technique uses UV-bright quasars as the background sources (for a recent review see Bechtold 2003). Many species have been detected in absorption, ranging from H I and He II, to Fe II and Zn II, plus high-ionization ions such as C IV and Si IV (e.g., Prochaska et al. 2001).

We examine the first ionization states of hydrogen and helium; they are the most abundant elements in the IGM, and are responsible for most of the UV opacity toward high-redshift quasars. Specifically, we will investigate the relative neutral fractions of hydrogen and helium, which have first ionization potentials of 13.6 and 24.6 eV, respectively. Since the photoionization cross-sections for H I and He I are peaked at threshold, their relative neutral fractions constrain the effective slope of the ionizing background between 13.6 and 24.6 eV.

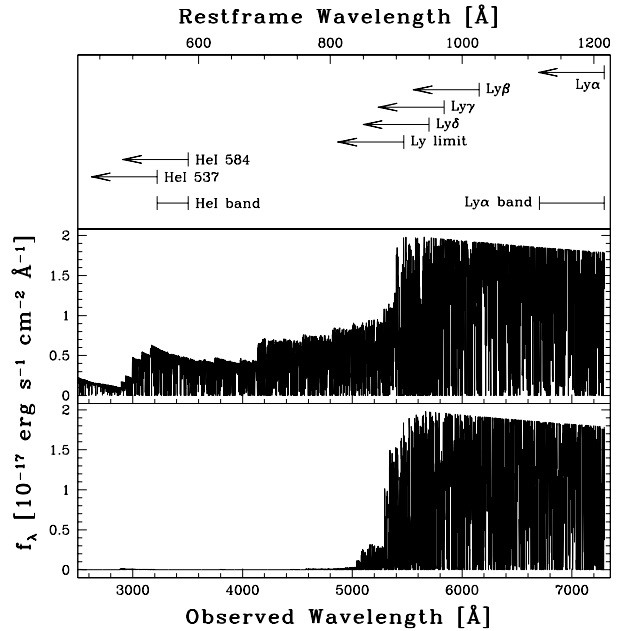


Figure 1. Simulated absorption spectra for $z = 5$ quasars with $AB_{1450} = 20$. The top axis is labelled in rest-frame wavelength, and the bottom axis is labelled in the corresponding observed wavelength at $z = 5$. The top panel shows the wavelengths where the first four Lyman series line forests begin; it also shows where the first two ground-state He I transition opacities begin. The He I band is shown, as is the region of the corresponding Ly α forest. The middle panel shows a quasar spectrum processed by IGM absorption, along a line-of-sight with relatively little IGM opacity. The bottom panel shows a quasar absorption spectrum along a typical line-of-sight.

The relative abundances of H I and He I constrain the ionizing background—the challenge is to measure these abundances in the IGM at high redshift. Both atoms exhibit line and continuum absorption. For H I, the Lyman series lines begin at 1216 Å and continue down to 912 Å, where continuous photoelectric absorption begins. The corresponding line transitions in He I are from $1s^2$ to $1s2p$ (584 Å), $1s3p$ (537 Å), etc., down to the first ionization threshold of helium, at 504 Å. These wavelengths are the rest-frame values; the observed wavelengths of these transitions depend on the redshift of the absorbing gas. If the neutral gas is distributed in many systems with a discrete redshift distribution, then the associated absorption lines appearing in a quasar spectrum form a ‘forest’ of absorption features against the continuum. Figure 1 shows two example absorption spectra with the general absorption regions labelled.

The absorption cross-sections of H I and He I are larger at the center of a line (at the IGM temperature of $\sim 2 \times 10^4$ K) than in the continuous absorption region. Despite this fact, the strongest absorption effect for the expected distribution of neutral IGM gas (see Section 4) is from the cumulative continuous absorption due to many absorbers at different redshifts, named the ‘valley’ by Møller & Jakobsen (1990). This is illustrated for H I in Fig. 1; once Lyman limit absorption begins (shortward of $912(1 + z_Q)$ Å, where z_Q is the quasar redshift), the forest typically gives way to almost complete absorption. In such cases it is very difficult to observe helium forest lines because of the small residual

continuum flux at short wavelengths. In rare cases the valley is not very pronounced, and the continuum is strong enough that the He I 584 Å forest region may be observed. We call the region of the He I 584 Å forest red-ward of He I 537 Å the ‘He I band.’

The identification of absorption features in spectra like those in Fig. 1 can be difficult, especially in low-resolution spectra, except in the region red-ward of the Ly β forest, where the only possible absorption feature from hydrogen or helium is the hydrogen Ly α line. (Trace metals produce additional absorption features, though these can be discriminated based on linewidth or because they have a doublet feature, e.g., C IV.) The He I band is the analogous region for He I, where the He I 584 Å lines are the only source of helium opacity; however, this region also may contain absorption due to all of the H I Lyman transitions, confusing the assignment of any individual line to He I. In principle, unsaturated He I lines could be identified because they are twice as narrow as unsaturated Ly α lines. However, line blending and the expected weakness of the He I lines complicate a practical implementation of that criterion, and spectroscopy of sufficiently high resolution would require an extremely bright target.

Even after hydrogen reionization is complete at $z \simeq 6$, the filamentary nature of the clumpy IGM leads to significant Ly α opacity in regions with neutral hydrogen column density of $N_{\text{HI}} \sim 10^{14} \text{ cm}^{-2}$. A line of sight through the universe pierces many of these filaments at different redshifts, resulting in the Ly α forest described above. Helium is expected to be singly reionized (24.6 eV ionization threshold) at a similar redshift to hydrogen, for almost any expected ionizing spectrum. Consequently, absorption by neutral helium at $z < 6$ should be confined to the same filaments that give rise to hydrogen absorption.¹ This justifies a one-to-one search for He I 584 Å lines at the same redshift as lines identified in the ‘Ly α band’ region, where the Ly α band is defined as the spectral region where absorbers with a He I 584 Å line in the He I band exhibit Ly α absorption (see Fig. 1).

The application of absorption line studies of the IGM is limited by the supply of suitable background sources, primarily quasars. The Sloan Digital Sky Survey² (SDSS) is a large photometric and spectroscopic survey of the northern sky that will identify and measure redshifts for almost all quasars brighter than 20th magnitude over one quarter of the sky. At the current discovery rate of the survey, it will find approximately 1000 quasars at $4 < z < 5.2$, and about 200 at $4.8 < z < 5.2$ (Anderson et al. 2001; Fan et al. 2001b). As we will demonstrate (Section 7), rest-frame extreme ultraviolet (EUV) absorption line study of $z \simeq 5$ quasars requires a large sample of quasars, and could only be realized with the large catalog of $z \simeq 5$ quasars that the SDSS will provide.

¹ This is in contrast to doubly ionized helium, which is distributed more diffusely (that is, the absorption features traces smaller over-densities) than hydrogen (Kriss et al. 2001).

² <http://www.sdss.org>

3 IONIZING BACKGROUND

Next we consider the relationship between the ionization state of IGM absorbers and the ionizing background. The quantity of interest for an absorbing system is the ratio of column density of neutral helium, N_{HeI} , to the column density of neutral hydrogen, N_{HI} ,

$$\eta \equiv \frac{N_{\text{HeI}}}{N_{\text{HI}}}. \quad (1)$$

As we will describe in Section 4, the abundance of absorbers as a function of redshift and N_{HI} is already observed. Thus predictions for He I absorption from these systems can be easily made from calculations of the relative ionization states of helium and hydrogen.

First we assume that the relative abundance of neutral helium to neutral hydrogen in an absorbing system with high H II and He II fractions³ is described by the optically-thin limit (e.g., Miralda-Escudé & Ostriker 1992),

$$\eta_{\text{thin}} \equiv \frac{N_{\text{HeI}}}{N_{\text{HI}}} = \frac{n_{\text{HeII}} \alpha_{\text{HeI}} \Gamma_{\text{HI}}}{n_{\text{HII}} \alpha_{\text{HI}} \Gamma_{\text{HeI}}} \simeq 0.083 \frac{\Gamma_{\text{HI}}}{\Gamma_{\text{HeI}}}, \quad (2)$$

where $n_{\text{He}}/n_{\text{H}} \simeq 0.083$ is the cosmic abundance ratio of helium to hydrogen (assuming a mass fraction of ${}^4\text{He}$ of 0.25, consistent with the combination of *WMAP* CMB results (Spergel et al. 2003) and big bang nucleosynthesis predictions (Burles et al. 2001)), $\alpha_{\text{HeI}}/\alpha_{\text{HI}} = 1.0$ is the ratio of the radiative recombination coefficients for He I and H I (Osterbrock 1989), and

$$\Gamma_{\text{HI}} = \int_{\nu_{\text{HI}}}^{\infty} d\nu \frac{4\pi J_{\nu} \sigma_{\text{HI}}(\nu)}{h\nu}, \quad (3)$$

and similarly for Γ_{HeI} . The angle-averaged specific intensity is J_{ν} , $\sigma_i(\nu)$ is the photoionization cross-section of species i , and the lower limit of the frequency integral is ν_i , the photon frequency at the ionization threshold of species $i = \text{H, He}$.

The most important absorbers for measuring η are systems where the observed equivalent widths of the Ly α forest absorption lines are roughly equal to the spectral resolution obtained in the Ly α forest spectrum. For a typical spectral resolution of 0.27 Å (a choice justified in Section 6.2), this corresponds to $N_{\text{HI}} \simeq 3 \times 10^{14} \text{ cm}^{-2}$ at $z \sim 5$. At such column densities, the optical depth to photons at the hydrogen ionization threshold is $\tau_{\text{HI}} \lesssim 2 \times 10^{-3}$, thus the optically-thin approximation should be valid.

However, optically thick absorbers can have a substantial impact on the spectrum of the ionizing background, both through absorption and emission. Haardt & Madau (1996) find that the mean UV background is attenuated by roughly a factor of 3 at both ν_{HI} and ν_{HeI} ; additionally, much of the flux shortward of 228 Å is absorbed by He II and re-emitted at 304 Å (see Haardt & Madau 1996, fig. 5c). These changes to the unabsorbed spectrum have important implications for the He III abundance, but do not affect the abundance ratio of He I to H I.

³ We neglect the possible presence of He III in the absorption systems. Observations suggest that the second reionization of helium did not occur until $z \simeq 3$ (Kriss et al. 2001; Theuns et al. 2002), and Wyithe & Loeb (2003b) predict that the full helium reionization happens over a narrow redshift interval. These studies suggest that most of the intergalactic helium was singly ionized at $z \simeq 5$.

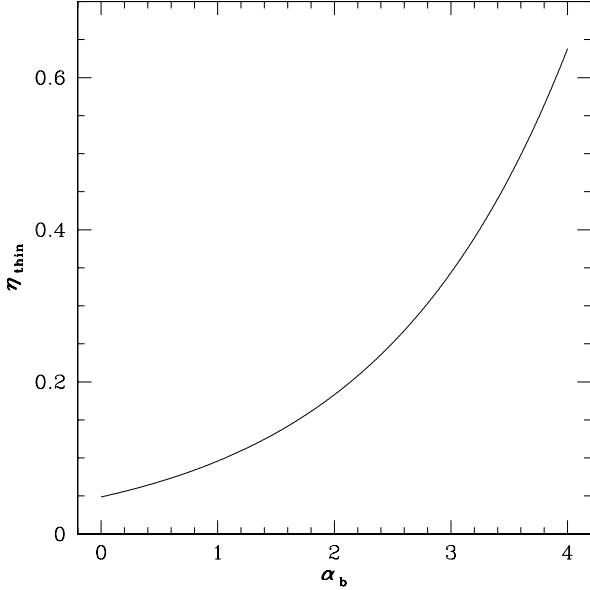


Figure 2. The ratio, η_{thin} , of the column density of neutral helium to the column density of neutral hydrogen, as a function of the spectral slope of the ionizing background, α_b . We assume that the absorbing systems are optically thin to ionizing radiation, highly ionized in hydrogen and highly singly-ionized in helium. The effective power-law index of a normal stellar population is $\alpha_b = 2.05$; the effective power law index of a population of very massive metal-free stars is $\alpha_b = 0.28$.

Because we are only concerned with the relative rate of neutral-helium ionizations to hydrogen ionizations, we approximate the ionizing background by a power law,

$$J_\nu \propto \nu^{-\alpha_b}. \quad (4)$$

Using a continuous star-formation history with metallicity $Z = 10^{-3}$ and a Salpeter IMF from 1 to $100 M_\odot$ (Leitherer et al. 1999), the effective power-law index is $\alpha_b = 2.05$. Also of interest is the spectrum of very massive metal-free stars, which represent the most extreme expectation of the stellar IMF at very high redshift: these stars are well approximated by a blackbody spectrum with temperature $T = 10^5$ K (Bromm, Kudritzki & Loeb 2001). Very massive metal-free stars yield a particularly hard power-law index of $\alpha_b = 0.28$. Quasars produce a spectrum with a power-law shape matching their own EUV spectral slope; that value is not well constrained at high redshift, but $\alpha_b = 1.6$ may be a reasonable guess (see Section 5). Finally, x-rays radiated from early stars have a near-zero spectral slope (Oh 2001), but the effect of secondary ionizations should produce an effective slope slightly greater than zero (S.P. Oh, private communication). Figure 2 shows the value of η_{thin} as a function of α_b .

4 IGM ABSORPTION MODEL

Our model for the H I absorption in the IGM is empirical, based on the data obtained in many quasar absorption line studies. Ongoing and planned observations are likely to constrain its parameters better in the future.

Absorption by H I is quantified by discretizing the absorption into individual absorbing systems, identified by their redshift, z , and neutral hydrogen column density, N_{HI} . The distribution of H I systems may be described reasonably well by power laws in both redshift and column density. We define H I systems with $N_{\text{HI}} < 1.6 \times 10^{17} \text{ cm}^{-2}$ as Ly α forest systems, and systems with $N_{\text{HI}} \geq 1.6 \times 10^{17} \text{ cm}^{-2}$ as Lyman Limit Systems (LLSs). The distribution of H I systems in redshift and column density are parametrized by three constants: A , γ , and s ,

$$\frac{dN(z)}{dz} = A(1+z)^\gamma, \quad (5)$$

$$f(N_{\text{HI}}) \propto N_{\text{HI}}^{-s}. \quad (6)$$

Here $N(z)$ is the total number of absorbers along a line of sight to redshift z , and $f(N_{\text{HI}})$ is the number of absorbing systems per unit H I column density.

We chose $s = 1.5$ for the power law index of the N_{HI} distribution for all values of N_{HI} , and assume that the absorber population extends up to $N_{\text{HI}} = 10^{22} \text{ cm}^{-2}$ (Storrie-Lombardi & Wolfe 2000). For the Ly α forest, we adopt the redshift evolution determined by *HST* observations at low redshifts (Dobrzycki et al. 2002, cf. Weymann et al. 1998) and from ground-based surveys at high redshifts (Bechtold 1994). Those surveys covered the H I column density range of $10^{14} \text{ cm}^{-2} \leq N_{\text{HI}} \leq 1.6 \times 10^{17} \text{ cm}^{-2}$ (i.e., from a rest-frame equivalent width of 0.24 \AA up to the LLSs). We extend their results to $N_{\text{HI}} = 10^{13} \text{ cm}^{-2}$ by scaling up the number density using the N_{HI} distribution quoted above, to give

$$\begin{aligned} A &= 106, & \gamma &= 0.65, & \text{for } z < 2.4, \\ A &= 29, & \gamma &= 1.7, & \text{for } z \geq 2.4. \end{aligned} \quad (7)$$

The transition redshift, $z = 2.4$, was chosen to match the low-redshift and high-redshift fits smoothly; this is higher than the traditional value of about 1.5 (e.g., Weymann et al. 1998), but is a consequence of the upward revision of γ by Dobrzycki et al. (2002) compared to Weymann et al. (1998); given the large uncertainties in the values of A and γ , this is not alarming.

For the LLSs, we adopt $A = 0.2$ and $\gamma = 1.5$, which are consistent with the results of Storrie-Lombardi et al. (1994) and Stengler-Larrea et al. (1995). We note that Stengler-Larrea et al. (1995) do not present an analysis of their full sample of LLSs because they exclude absorption systems within 5000 km s^{-1} of the quasar, yet their results are consistent with the result of Storrie-Lombardi et al. (1994) for all LLSs. These parameter choices provide a relatively smooth intersection between the abundance of LLSs and Ly α forest systems at $z \geq 1$, assuming the column density distribution described above. The covariance of the uncertainties in A and γ implies that the mean number of LLSs toward a high-redshift quasar is constrained, but the LLS distribution with redshift is uncertain: the $1\text{-}\sigma$ uncertainty on γ is about 0.4 (Storrie-Lombardi et al. 1994; Stengler-Larrea et al. 1995).

The absorber distributions described above can be converted into a mean comoving H I number density using

$$\langle n_{\text{HI}}^c(z) \rangle = A(1+z)^\gamma \frac{H_0 E(z)}{c(1+z)^2} \langle N_{\text{HI}} \rangle, \quad (8)$$

where H_0 is the Hubble constant, $\langle N_{\text{HI}} \rangle$ is the mean H I column density of the absorber population, and

$$E(z) = [\Omega_{\text{m}}(1+z)^3 + \Omega_{\Lambda} + (1 - \Omega_{\text{m}} - \Omega_{\Lambda})(1+z)^2]^{1/2}. \quad (9)$$

For a universe with density parameters $\Omega_{\text{m}} = 0.3$ in matter, $\Omega_{\Lambda} = 0.7$ in a cosmological constant, and $\Omega_{\text{b}} h^2 = 0.02$ in baryons, and a Hubble constant $h \equiv H_0 / (100 \text{ km s}^{-1} \text{ Mpc}^{-1}) = 0.7$, this gives an H I neutral fraction at $z \gtrsim 4$ of,

$$\langle x_{\text{HI}}(z) \rangle \simeq 9.8 \times 10^{-3} A (1+z)^{\gamma-1/2} \frac{\langle N_{\text{HI}} \rangle}{4 \times 10^{19} \text{ cm}^{-2}}. \quad (10)$$

For LLSs (which have $\langle N_{\text{HI}} \rangle = 4 \times 10^{19} \text{ cm}^{-2}$), $A = 0.2$ and $\gamma = 1.5$, thus $\langle x_{\text{HI}}(z=6) \rangle = 0.01$. This is consistent with the limit derived by Fan et al. (2002) from H I absorption toward a $z = 6.28$ quasar.

We assume that there is no correlation between absorbing systems. There is observational evidence for clustering of the Ly α forest lines (e.g., Liske et al. 2001; Dobrzycki et al. 2002, and references therein), but our assumption is conservative for the purposes of this paper: we will show that to study He I absorption, we need quasars with fewer than average absorbers along the line of sight. Clustering of absorbers would skew the ‘bad’ quasar targets (i.e., those with many strong absorbers) worse, and skew the ‘good’ quasar targets better. This is not an important effect for low- N_{HI} absorbers, since they are very numerous, but could be a significant effect for LLSs if they are clustered (note, however, that Sargent, Steidel, & Boksenberg 1989 showed that LLSs followed Poisson statistics in their sample of 37 absorbers). The proximity effect generates an absorber deficit of ~ 30 per cent within $4 h^{-1} \text{ Mpc}$ of the quasar, or about 200 \AA observed from the quasar Ly α line (Scott et al. 2000). We also ignored this relatively small effect.

In addition to the absorber redshift and column-density distributions, our IGM model must also describe their absorption properties. We used the photoionization cross-sections given by Osterbrock (1989) for H I and Verner et al. (1996) for He I. Our model treats the first 11 line transitions from the ground state (which all atoms are assumed to occupy), using data from the NIST Atomic Spectra Database v2.0.⁴ The line profiles were modelled as Doppler cores of width $b = 26 \text{ km s}^{-1}$ (Kim et al. 1997) with damping wings outside of the core (e.g., Peebles 1993).⁵

Our absorption model includes only hydrogen and helium; metal lines are not considered here. There are not likely to be many metal line systems in the quasars used to measure η because metal lines are associated with H I absorbers of high column density, and, due to the selection techniques employed (see Section 6), quasars with strong absorbing systems are unsuitable for measuring η . Moreover, the strongest metal lines that could pollute the Ly α band, such as the C IV and Mg II doublets, show only a few absorbers per unit redshift, compared to of order 100 Ly α absorbers in the same redshift interval. In the He I band, metal lines are again far less numerous than H I lines, and thus were ignored.

⁴ http://physics.nist.gov/cgi-bin/AtData/main_asd

⁵ In Section 6.2 we assume instrumental resolutions considerably larger than 26 km s^{-1} , so the choice of exactly that value and our use of a single b value for all absorbers rather than the actual distribution should have a negligible effect on our results.

One complication to the application of absorber statistics determined from other quasar samples to the population of quasars discovered by SDSS is the quasar selection techniques employed. The SDSS quasar selection primarily uses observed optical colors to generate a well-defined selection function (Fan et al. 1999); by contrast, the quasars studied in absorption line surveys were culled from heterogeneous catalogs (e.g., Hewitt & Burbidge 1987), and include radio-, x-ray-, and emission-line-selected quasars in addition to color-selected quasars. An analysis of the systematic errors introduced by using absorption lines in quasars discovered by several different techniques to predict absorption patterns in quasars selected by another technique is outside the scope of this paper; we simply analyze the colors of the quasars most important to this study to ensure they would meet the quasar color-selection criteria of SDSS (see Section 7).

5 MODEL QUASAR INTRINSIC SPECTRUM

In order to simulate realistic observations of IGM absorption of background quasars, we need to make assumptions about the intrinsic properties of the quasar UV spectrum. The SDSS will provide a large catalog of high-redshift quasars, so we attempt to model the typical properties expected of SDSS quasars based on the results of the survey so far.

In a sample drawn from 182 square degrees of the SDSS, Fan et al. (2001a) presented 18 quasars with $z \geq 4$ and $i^* < 20$, where i^* is the preliminary SDSS determination of the quasar i' magnitude. We assume the quasars presented are a fair sample of the final SDSS results.

For each quasar in their sample, Fan et al. (2001a) compute the properties of the quasar near-UV (NUV) continuum, assuming a power law form, $f_{\nu} \propto \nu^{-\alpha_{\text{NUV}}}$. They set the normalization to the quasar continuum at the observed wavelength corresponding to rest-frame 1450 \AA . They then convert that specific flux into a magnitude on the AB system,

$$\text{AB}_{1450} = -2.5 \log_{10} [f_{\nu}(\lambda_{\text{rest}} = 1450 \text{ \AA})] - 48.6, \quad (11)$$

where $f_{\nu}(\lambda_{\text{rest}} = 1450)$ is the specific flux in $\text{erg s}^{-1} \text{ cm}^{-2} \text{ Hz}^{-1}$ at rest-frame 1450 \AA . Typically $\text{AB}_{1450} \simeq i^*$ or z^* , depending on quasar redshift. Fan et al. (2001a) also estimate α_{NUV} for each quasar; the mean for quasars with $z \geq 4$ is 0.6, with substantial uncertainty in the slope of any individual quasar. However, Telfer et al. (2002) found a break in the UV slope of their quasar composite spectrum near the wavelength of Ly α ; the measured slope became softer blue-ward of Ly α . This confirmed earlier work by Zheng et al. (1997). The Telfer et al. (2002) sample is comprised almost entirely of quasars with $z < 2.5$; for radio-quiet quasars they find a mean EUV slope of about 1.6, with a break to a shallower NUV slope at about 1250 \AA . Telfer et al. (2002) compare their radio-quiet sample to the radio-quiet SDSS quasar sample of Vanden Berk et al. (2001), and find an evolution toward harder NUV slope with samples at higher redshift; EUV comparison between the samples is extremely difficult due to the presence of strong IGM absorption in the high-redshift quasars.

Given the available observational evidence, we adopt a conservative model for the EUV properties of SDSS quasars: $\text{AB}_{1450} = 20$ with a NUV slope of 0.6 between rest-frame

1450 and 1250 Å and an EUV slope shortward of 1250 Å given by $\alpha_{\text{EUV}} = 1.6$.

6 LINES OF SIGHT TOWARD SDSS QUASARS

Many $z \sim 5$ quasars will be discovered by SDSS; in this Section we evaluate how good the best quasar target will be. We then simulate observations of the best quasar target and demonstrate our ability to constrain the spectrum of the ionizing background from such data.

Extrapolating from the results of the color-selected sample of Fan et al. (2001a), SDSS will discover ~ 1000 quasars with $4 < z < 5.2$. We assume the SDSS quasar selection function does not depend much on redshift over the range $4 < z < 5.2$; this is a conservative estimate for our purposes because the detection probability is higher for quasars with $4.7 < z < 5.2$ than for other $z > 4$ quasars (Fan et al. 2001a). Fan et al. (2001b) fit the redshift dependence of the high redshift quasar spatial density with $\rho \propto 10^{-0.5z}$. Thus about 200 of the high-redshift quasars will fall within the range $4.8 < z < 5.2$.

We would like to know how many of these quasars have spectra like the middle panel of Fig. 1, which would be useful for measuring He I lines, and how many have spectra like the bottom panel of Fig. 1, which would not be a suitable target for measuring He I lines. We quantify this by determining the distribution of quasar sightline ‘suitability,’ as measured by the flux of the quasar in the He I band. From that distribution and the expected number of SDSS quasars, we determined what the most suitable quasar discovered by the SDSS will be. Though for some applications an analytic approach to the subject is suitable (Zuo & Phinney 1993), we require a Monte Carlo simulation approach (Møller & Jakobsen 1990; Jakobsen 1998) for this study.

6.1 Absorber Monte Carlo simulations

We started from the distribution of H I absorbing systems in redshift and column density described in Section 4. For a quasar at a given redshift z_Q , we used Poisson statistics to generate the number of low- z Ly α forest, high- z Ly α forest and LLS absorbers along the line of sight. Once we generated the number of absorbers of each type, we assigned redshifts and column densities drawn from the absorber model described in Section 4. This list of absorbers was then passed through a routine to calculate the optical depth to H I at every sampled wavelength value.⁶ In each simulated spectrum, the optical depth due to helium was stored separately from hydrogen; given the universal optically thin ratio of column densities, η_{thin} derived in Section 3, the helium optical depth scales simply as η_{thin} .

For each LOS, the H I optical depth data were converted into the IGM transmission as a function of wavelength. We integrated the IGM transmission over the He I

⁶ Wavelength sampling ranges from 0.08 to 0.28 Å, chosen so that there are three samples per Doppler FWHM of the spectral lines of interest (He I lines are twice as narrow as H I lines); all results were checked for sensitivity to spectral resolution and are converged at this resolution choice.

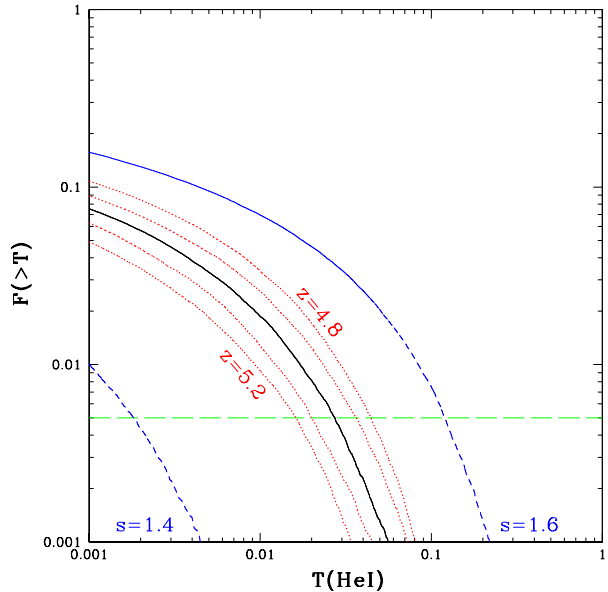


Figure 3. Cumulative histogram of the He I-band transmission along quasar lines-of-sight, as a function of redshift and absorber model. The solid curve shows the fraction of $z = 5$ quasars that have a mean transmission in the He I band greater than a given mean transmission value $T(\text{He I})$, assuming $s = 1.5$ in the distribution of absorber column densities (Section 4). The lowest dashed curves are for $s = 1.4$ and $s = 1.6$, respectively, assuming $z = 5$ quasars. The two dotted curves closely above the solid curve are for $z = 4.9, 4.8$, and the two dotted curves closely below the solid curve are for $z = 5.1, 5.2$, all assuming $s = 1.5$. The horizontal dashed line at $1/200$ intersects the curves at the expected $T(\text{He I})$ of the best quasar in a sample of 200 quasars.

band to derive the mean He I-band transmission along each LOS, $T(\text{He I})$. Figure 3 shows the cumulative fraction of quasars with $T(\text{He I})$ greater than a given value. For simplicity, we will assume the expected 200 SDSS quasars with $4.8 < z_Q < 5.2$ all fall at $z_Q = 5$. Then from Fig. 3 we can read off the value of $T(\text{He I})$ corresponding to a fraction of $1/200$; this is the largest expected $T(\text{He I})$ value of the lines-of-sight toward the SDSS quasars. The result is $T(\text{He I}) = 0.03$. Note that if we change the assumed redshift of the quasars by $\Delta z = 0.2$ (the dotted lines in Fig. 3), the expected maximum value of $T(\text{He I})$ for 200 quasars changes by a factor of about 2. When the final SDSS quasar catalog is constructed, we may use the real distribution of quasar redshifts together with our simulation machinery to generate a $T(\text{He I})$ histogram that depends only on the IGM absorber model. Thus measurements of the observed distribution of $T(\text{He I})$ can be used to constrain a combination of the properties of the H I component of the IGM and the intrinsic quasar spectral shape.

Small changes to the absorber-model parameter s , the slope of the column-density distribution, have a strong effect on the expected maximum value of $T(\text{He I})$ (as pointed out by Møller & Jakobsen 1990, and illustrated by the dashed lines in Fig. 3). In the next subsections we discuss what could be learned about the $z \simeq 5$ ionizing background under the assumption that SDSS will discover a quasar with properties given in Section 5 along a LOS with $T(\text{He I}) = 0.03$, our

‘expected’ value for the best SDSS quasar, or $T(\text{HeI}) = 0.1$, which we consider to be a reasonable ‘optimistic’ value for the best SDSS quasar.

6.2 Quasar absorption line spectrum simulations

Based on the results of the previous subsection, we analyzed lines-of-sight with $T(\text{HeI}) = 0.03$ and 0.1 , our ‘expected’ and ‘optimistic’ values for the best SDSS quasar LOS. For each observational realization of a quasar along the simulated LOS, a value of η was assumed. Then the optical depth data were used to construct the IGM transmission as a function of wavelength. This was multiplied by the intrinsic quasar spectrum from the model described in Section 5 to generate the observed spectrum. The Galactic extinction curve was taken from Scheffler & Elsässer (1988). Atmospheric extinction was applied based on the sky transparency from Mauna Kea (the location of the Keck Observatory).⁷ Our modelling of the telescope and instrument parameters included slit losses, system throughput, instrumental resolution, pixel sampling, spatial extraction of the spectra, and detector noise. Slit losses and spatial extraction both incorporate an assumed value for the seeing. A mean emission spectrum of the sky,⁸ measured at Mauna Kea, was also passed through the telescope/instrument model.

Our model observations were performed assuming a Galactic extinction value of $A_{V'} = 0.15$ toward the target quasar, typical for SDSS quasars (Schneider et al. 2002). We assumed the observations were made at a constant value of 1.2 airmasses and a constant seeing of 0.7 arcsec.

Our simulated observations of the H I Ly α forest were based on the properties of the Keck II 10-meter telescope and the Echellette Spectrograph and Imager (ESI; Sheinis et al. 2002), an intermediate resolution optical spectrograph, with ESI in echelle mode ($R \sim 4000$). We assumed a 1 arcsec slit, with 75 km s^{-1} resolution and $11.5 \text{ km s}^{-1} \text{ pixel}^{-1}$. The spatial extraction window was 0.77 arcsec; the spatial pixel scale was $0.154 \text{ arcsec pixel}^{-1}$. We assumed no dark current, and a readnoise of 2.1 counts per pixel (the gain was 1.3 e^- per count). We assumed each H I Ly α forest spectrum consisted of 40 co-added 1000 sec observations, for a total exposure time of 11 hours. This is similar to the exposure times of Keck observations of the highest-redshift SDSS quasars (White et al. 2003).

We assumed that the He I band was observed with the Keck I 10-meter telescope and the Low-Resolution Imaging Spectrometer (LRIS; Oke et al. 1995), using the blue channel of LRIS (LRIS-B; McCarthy et al. 1998) with the 1200 line grism. This configuration with a 0.7 arcsec slit delivers a resolution of 1.30 \AA , sampled at $0.24 \text{ \AA pixel}^{-1}$. The spatial extraction window was 1.08 arcsec, about 1.5 times the seeing; the spatial pixel scale was $0.2151 \text{ arcsec pixel}^{-1}$. We assumed no dark current, and a readnoise of 2.5 counts per pixel (the gain was 1.6 e^- per count). Because readnoise otherwise made a non-negligible contribution to the noise, we binned the data by 2 pixels in the spatial and spectral

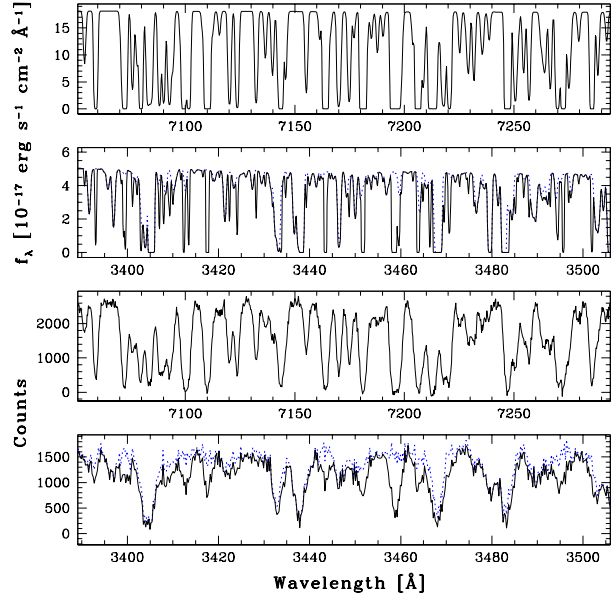


Figure 4. A simulated absorption spectrum for a $z = 5$ quasar with $AB_{1450} = 20$. The top panel zooms in on the $z = 4.8\text{--}5$ H I Ly α forest of the spectrum from the middle panel of Fig. 1. The second panel shows the corresponding $z = 4.8\text{--}5$ He I 584 \AA forest region of the same spectrum; the dotted curve is the absorption from H I only, and the solid curve assumes $\eta_{\text{thin}} = 0.5$ for illustration. The lower two panels show mock observations of the quasar, using the observation model described in Section 6.2.

directions. We assumed each He I 584 \AA forest spectrum consisted of 72 co-added 2000 sec observations, for a total exposure time of 40 hours. This is substantially more observation time than is typically devoted to any one object with Keck. However, the total observation time devoted to study He II absorption in the $z = 2.885$ quasar HE2347-4342 was almost 150 hours with the *FUSE* satellite.

For each simulated exposure, we computed the expected signal, expected sky, and expected detector noise. The observed counts in each spectral pixel due to source, sky and detector were drawn from Poisson distributions with the means set to the expected counts, and the three contributions were summed. Then the expected sky and detector noise were subtracted (assuming photon-noise limited sky subtraction). The simulated exposures were then summed to create the final simulated observation.

6.3 Quasar absorption line spectrum analysis

Our goal is to estimate the ionization state of the IGM as measured by the relative abundance of He I to H I, η . Our analysis technique is to make use of the cross-correlation of the H I Ly α forest spectrum and the He I-band spectrum, which depends on η as illustrated in Fig. 4.

Each pixel in the He I-band spectrum was matched up with the Ly α -band spectrum pixel whose wavelength is closest to $\lambda_{\text{HI}} = (1216/584)\lambda_{\text{HeI}}$, where λ_{HeI} is the wavelength of the He I-band pixel. Thus an absorber at a given redshift will exhibit He I 584 \AA absorption and Ly α absorption in matched pixels. Figure 5 shows a plot of the fluxes, normal-

⁷ http://www2.keck.hawaii.edu/inst/lris/atm_trans.html

⁸ <http://www.cfht.hawaii.edu/Instruments/ObserverManual/chapter5.html>; note the sky will darken slightly as we approach solar minimum in 2008.

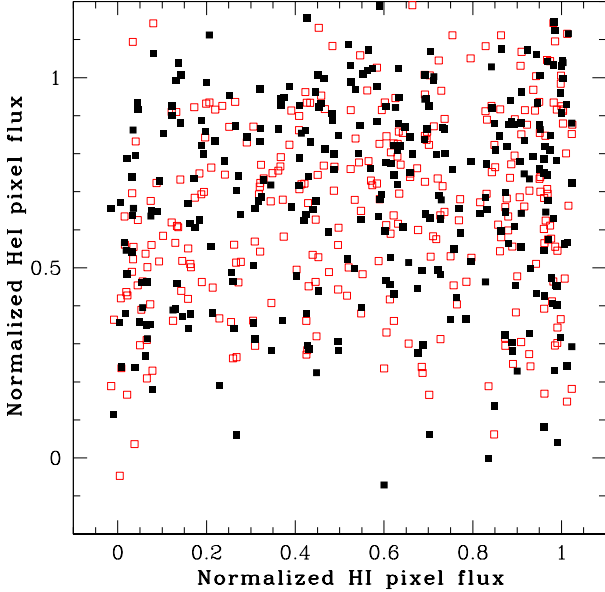


Figure 5. An example of the pixel-by-pixel cross-correlation of the absorption in the He I band and the H I Ly α band. The solid squares represent continuum-normalized flux pairs from an observation of a quasar LOS with $\eta = 0.06$; the open squares are from an observation of the same LOS but assuming $\eta = 0.20$.

ized to the local quasar continuum, of pixel pairs matched in this manner, for two values of η . If He I 584 Å absorption and Ly α absorption were the only features in the spectra, and the observations were perfect, then the points would fall along a tight locus described primarily by η . In regions of little absorption, both continuum-normalized pixel fluxes would be near one: regions of strong absorption would have normalized H I pixel fluxes near zero and normalized He I pixel fluxes set by η . However, the presence of other lines and the effects of instrumental smoothing and observational noise scatter the points. There is little scatter in the H I-pixel-flux direction, both because these simulated observations have a good signal-to-noise ratio, and because there are no absorption features in the Ly α band besides Ly α . There is substantial scatter in the He I-pixel-flux direction, though, because of lower signal-to-noise in the observations, and also the presence of Ly α absorption (and, to a lesser extent, absorption due to the other Lyman series lines) from low-redshift absorbers. Despite the scatter, one can easily see that, at low values for the normalized H I pixel flux, the points Fig. 5 for the $\eta = 0.06$ case (solid squares) lie higher (less He I absorption) than the points for the $\eta = 0.20$ case (open squares).

In the He I-band spectrum, we would like to know what the quasar effective continuum level is after accounting for bound-free absorption by higher-redshift absorbing systems. For a $z_Q = 5$ quasar, any strong absorber between $z = 2.53$ and $z = 2.84$ will cause a change in the effective continuum in the He I band, due to the H I bound-free absorption edge at $912(1+z)$ Å. Consequently, the H I Ly α forest spectrum should be searched for strong Ly α lines over the range of 4292 to 4669 Å (for $z_Q = 5$). We assumed for our analysis that the effective continuum can be accurately estimated. In

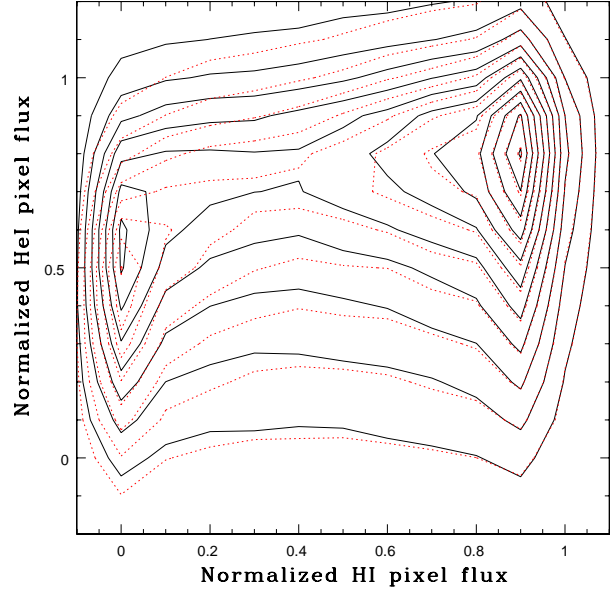


Figure 6. Contour plot of the ensemble continuum-normalized fluxes of pairs of corresponding He I-band and Ly α -band pixels (see Section 6.3). The solid contours assume $\eta = 0.06$, and the dotted contours are for $\eta = 0.20$. Pixel pairs with strong H I absorption have H I pixel fluxes near zero; for those pairs increasing η shifts the He I pixels to smaller fluxes, due to increased He I absorption associated with the H I absorption.

the analysis of real observations, one could apply the same technique used to estimate the effective continuum to our mock observations, and thus analyze the real observations in an unbiased way.

Using our large Monte Carlo library of simulated quasar LOSs, we generated the distribution of pixel pair fluxes, as a function of η , for multiple observational realizations of a quasar along each LOS. Figure 6 shows contours that represent the likelihood of finding a given pair of continuum-normalized fluxes for $\eta = 0.06$ and $\eta = 0.20$. This distribution of mock-observational results were then used to analyze an individual observation of a quasar LOS: we generated the matched pair data as shown in Fig. 5, then summed the value of the likelihood at that point over all the pixel pairs with continuum-normalized H I pixel fluxes less than 0.5 (cf. Fig. 6), for each of the two values of η under consideration. We termed each sum of the likelihood values (which depend on η) $L(\eta)$. The $L(\eta)$ value is larger when a set of pairs matches up well with the contours of Fig. 6 for η , and smaller when there is not a good match. Then we formed the ratio $R \equiv L(0.06)/L(0.20)$, which we find is better for recovering our input value of η than, for example, $L(0.06) - L(0.20)$. We have found that binning the He I-band spectra by 2 pixels (in addition to the 2×2 on-chip binning) reduces the scatter in R .

Figure 7 shows histograms of R for each of our two input values of η , assuming observations described in Section 6.2 of a quasar along a sightline with $T(\text{He I}) = 0.03$, our *expected* value for the best SDSS LOS toward a $z \simeq 5$ quasar (see Section 6.1). The histograms are clearly separated, though they do show some overlap. Figure 8 is the same as Fig. 7,

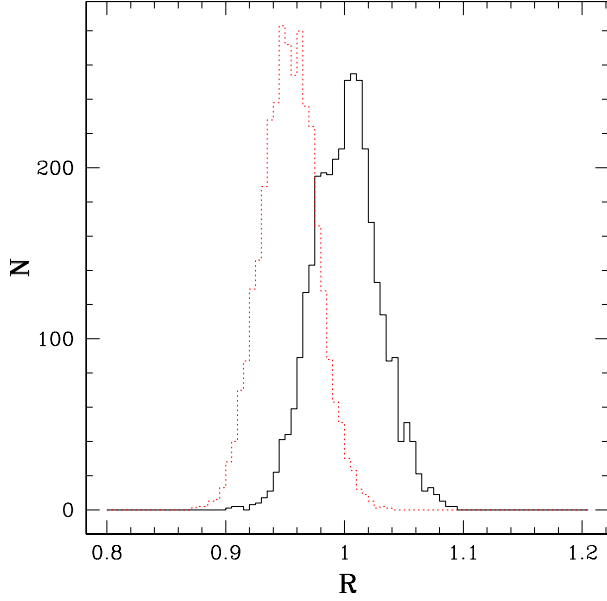


Figure 7. Histograms of R (see Section 6.3) for each of our two input values of η , 0.06 and 0.20, assuming observation of a quasar along a sightline with $T(\text{HeI}) = 0.03$. The solid (dotted) line shows the R histogram for analysis of quasar LOSs with $\eta = 0.06$ ($\eta = 0.20$).

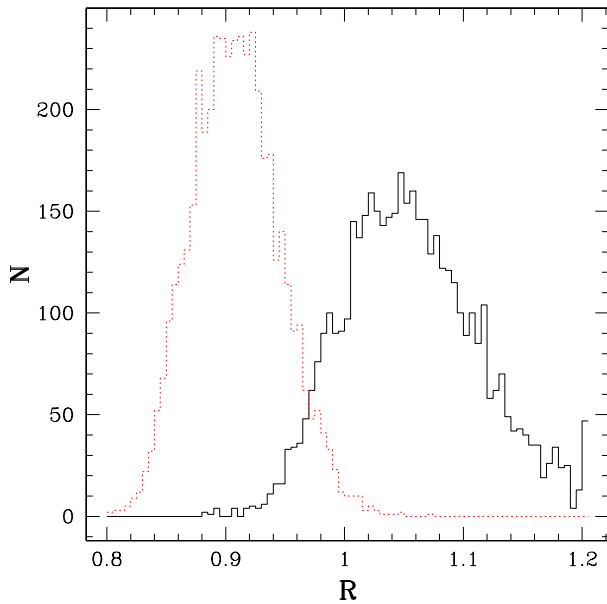


Figure 8. Same as Fig. 7 but for an LOS with $T(\text{HeI}) = 0.1$.

but for observations along a LOS with $T(\text{HeI}) = 0.1$, our *optimistic* value for the best quasar LOS in the SDSS. In this case the histograms are much more clearly separated, illustrating the importance of discovering a very good quasar LOS.

Figures 9 and 10 cumulate (and normalize) the histograms of Figs. 7 and 8. They illustrate that, for our model observations toward one $T(\text{HeI}) = 0.03$ LOS, if the true

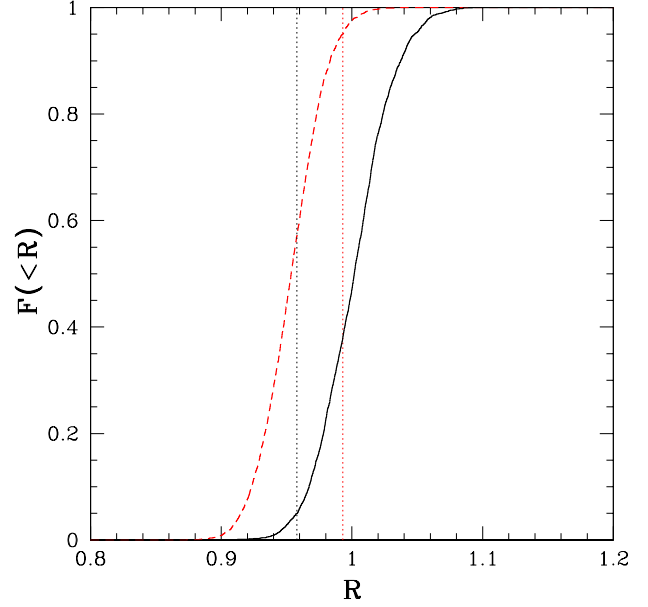


Figure 9. Normalized cumulative histograms of R from Fig. 7; 95 per cent of the LOSs have $R(0.06) > 0.958$, the position of the left vertical line, and 95 per cent of the LOSs have $R(0.20) < 0.993$, the position of the right vertical line. Thus if the intrinsic η value along a LOS is either 0.06 or 0.20, one observation has about a 60 per cent chance of rejecting the other value.

value of η is 0.06, then we have almost a 60 per cent chance of making an observation that will reject $\eta = 0.20$ at the 95 per cent confidence level. Conversely, if the true value of η is 0.20, then we have a 60 per cent chance of making an observation that will reject $\eta = 0.06$ at the 95 per cent confidence level. The situation along a $T(\text{HeI}) = 0.1$ LOS is much more optimistic: if the true value of η is either one of our model choices, we will reject the other value of η about 95 per cent of the time at the 95 per cent confidence level.

Using the observations we propose, it will be difficult to estimate a precise value of η from the data. If the true value of η is, for example, 0.11, then we will only be able to reject very extreme values of η . However, if the ionizing background is either hard or soft, it may well be possible to reject the other hypothesis. For example, if we measured an R value of 1, we could be confident that the ionizing background at $z \simeq 5$ is not dominated by Pop II stars.

7 OBSERVATIONAL QUASAR SELECTION TECHNIQUES

In previous Sections we estimated the likely properties of the best SDSS quasar for the measurement of He I absorption features, and what we could learn about the $z \simeq 5$ ionizing background from analysis of such a quasar. In this Section we describe the final aspect of practical implementation, how to pick out the best SDSS quasar from the expected sample of 200.

We would like to select the $z \simeq 5$ SDSS quasar with the highest flux in the He I band. So far we have primarily discussed $T(\text{HeI})$, the IGM-transmitted fraction in the He I band; however, this was always under the assumption

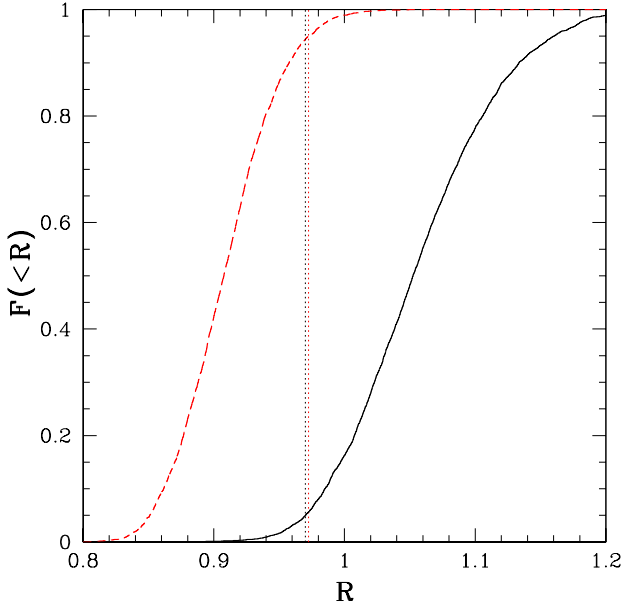


Figure 10. Normalized cumulative histograms of R from Fig. 8; 95 per cent of the LOSs have $R(0.06) > 0.970$, the position of the left vertical line, and 95 per cent of the LOSs have $R(0.20) < 0.972$, the position of the right vertical line. Thus if the intrinsic η value along a LOS is either 0.06 or 0.20, one observation has about a 95 per cent chance of rejecting the other value.

of the intrinsic quasar model described in Section 5. The real SDSS quasar sample will certainly include quasars with a range of values for AB_{1450} , and these quasars may have a range of EUV spectral shapes. Due to these distributions, the quasar with the largest He I-band flux may not be the quasar with the largest $T(\text{He I})$; we made conservative assumptions about AB_{1450} and the EUV spectrum, so we expect that the true distributions of quasar properties may only improve the suitability of the best SDSS quasar over our estimates.

For $z_Q = 5$, the He I band covers 3222 to 3506 Å; this is within the SDSS u' filter, which runs from ~ 3250 to 3750 Å (Fan et al. 2001a). As a consequence we expect the u' magnitude to serve as a good proxy for the He I-band flux. Figure 11 shows the relationship between $T(\text{He I})$ and $T(u')$, the transmitted flux fraction in the u' band. The strong correlation illustrated in the scatter plot is independent of the intrinsic quasar properties. Assuming our standard quasar model, the transmitted fractions are directly related to fluxes; the cumulative histogram at the bottom of Fig. 11 shows the fraction of observed quasars brighter than a given value of u' . We expect that 95 per cent of SDSS $z \simeq 5$ quasars will be fainter than $u' = 27$, but the quasar with the highest He I-band flux will have $u' \sim 25.5$, with an optimistic value of $u' = 24$. The u' -band $1\text{-}\sigma$ limiting magnitude for the SDSS survey is expected to be about $u' = 24$ (Fan et al. 2001a), thus under optimistic assumptions there is some chance the SDSS survey itself would make a u' detection of a $z \simeq 5$ quasar, and thus identify an excellent candidate for spectroscopic follow-up observations. It is likely, however, that deeper u' -band photometry on the SDSS quasars will be desirable to locate the few brightest

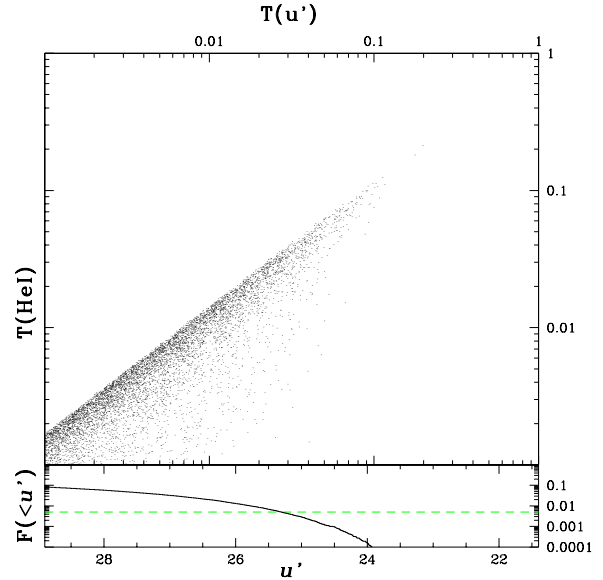


Figure 11. Plot of $T(\text{He I})$ versus $T(u')$. This plot shows the mean transmissions in the He I band and in the u' band for each $z = 5$ quasar LOS in 10^5 LOS Monte Carlo simulations. The excellent correlation between $T(\text{He I})$ and $T(u')$ at the high $T(\text{He I})$ end of the distribution shows that u' -band photometry is an effective method for selecting the best quasar for follow-up He I-band spectroscopy. Under the assumption that the intrinsic quasar spectrum is given by the model of Section 5, we convert $T(u')$ into a u' -band AB magnitude, and plot the cumulative fraction of quasars brighter than that magnitude in the bottom panel. The horizontal dashed line at $1/200$ intersects the curve at $u' = 25.3$, the expected u' magnitude of the brightest quasar in a 200 quasar sample.

quasars in the u' band. The 2.5-meter SDSS telescope integrates for only 54.1 seconds per filter, so achieving deeper u' photometry on a small telescope equipped with a blue-sensitive CCD should not be difficult (extending the $1\text{-}\sigma$ limit to $u' = 25.5$ would only require 2.5 minutes per source with the SDSS telescope, or about 8 hours of total integration time for all 200 SDSS $z \simeq 5$ quasars).

Once candidates have been identified from u' -band photometry, low-resolution spectroscopy should be performed to determine the flux in the He I band; because the u' band extends longward of the He I band, a quasar can be relatively bright in u' but faint in the He I band (note the points scattered below the main correlation in Fig. 11). The low-resolution spectroscopy will require a blue-sensitive spectrograph, but on only a 2-meter class telescope.

We now turn to our final point: the SDSS quasars are selected based on photometry in all of the SDSS bands. The primary SDSS photometric-selection criteria for $z \simeq 5$ quasars require $u' > 22.00$ and $g' > 22.60$ (Fan et al. 2001a). As illustrated in Fig. 11, we do not expect any $z \simeq 5$ quasars to be nearly as bright as $u' = 22.00$. In contrast, Fig. 12 shows that quasars with $T(\text{He I}) = 0.1$ will sometimes be slightly brighter than 22.60 in g' . Though unlikely, it is possible that the SDSS quasar selection algorithm could miss not only a $z \simeq 5$ quasar, but the best one in the survey for our purposes. When the SDSS quasar survey is complete,

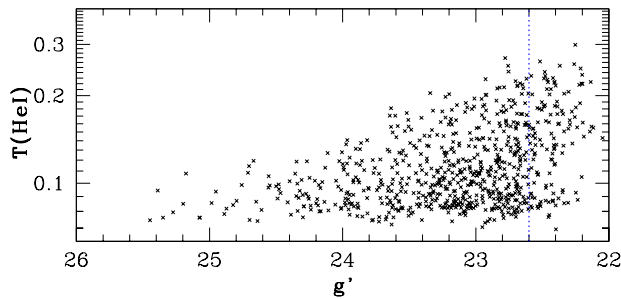


Figure 12. Plot of $T(\text{He I})$ versus g' of quasars. These points are for the standard intrinsic quasar flux model of Section 5. Only quasars with $g' > 22.60$ (plotted to the left of the dotted line) are identified by the SDSS quasar color selection algorithm as quasars. Note that this plot focuses on quasars with very optimistic values of $T(\text{He I}) \gtrsim 0.1$; quasars with lower values of $T(\text{He I})$ generally all fall at $g' > 22.60$.

and the SDSS data are publicly released, a full search of the SDSS catalog can be made to determine whether any objects meet all the SDSS $z \simeq 5$ quasar criteria except for $g' > 22.60$, but still have, e.g., $g' > 22.40$. These objects could be followed up independently.

8 SUMMARY

We have developed a method to infer the dominant stellar population responsible for the ionizing background radiation at $z \simeq 5$, using absorption lines in the spectrum of a $z \simeq 5$ quasar. Specifically, we related the strength of relative absorption in He I lines compared to H I lines to whether Pop II or Pop III stars dominated the ionizing background shortly after reionization completed.

First we related the ionizing background shape to the ratio, η , of He I to H I in an optically thin absorbing system; the spectrum of Pop II stars gives rise to $\eta = 0.20$ while the spectrum of very massive Pop III stars yields $\eta = 0.06$. Then we adopted a model for the population of IGM absorbers based on absorption line observations of quasars. The existing observations do not tightly constrain absorber populations at $z \gtrsim 4$; our model does extrapolate to a neutral fraction of 1.4×10^{-2} at $z = 6.28$, consistent with measurements. We adopted a model quasar spectrum to shine through our model IGM: we assumed the quasar flux to be at the faint limit for the SDSS quasar survey (20th magnitude in the AB system at rest-frame 1450 \AA), and modelled the EUV spectral shape based on the composite spectrum of lower-redshift quasars with a spectral slope of $\alpha_{\text{EUV}} = 1.6$.

We extrapolated the early results of the SDSS quasar survey to find that SDSS will discover 200 quasars with $4.8 < z < 5.2$. We used Monte Carlo simulations of our IGM model to generate random realizations of lines-of-sight (LOSs) toward $z_{\text{Q}} \simeq 5$ quasars. Based on those results, we concluded that a sample of 200 quasars should contain one quasar along a line-of-sight with 3 per cent transmission by the IGM in the He I band ($537(1+z)$ to $584(1+z) \text{ \AA}$); given the uncertainty in the absorber model, we consider a LOS with 10 per cent transmission to be an optimistic possibility.

We simulated large numbers of quasar LOSs with 3 and

10 per cent transmission. We placed a model quasar at $z = 5$, and then simulated observations of the He I and H I forests. Based on the result for a large ensemble of observations, we derived an estimation technique that can discriminate (at 95 per cent confidence) a Pop II ionizing background from a Pop III ionizing background ~ 50 per cent of the time for observations along our *expected* best LOS, and that can discriminate the backgrounds 95 per cent of the time for observations along our *optimistic* best LOS. These observations require very long integrations with a 10-meter class telescope instrumented with a blue-sensitive low-dispersion spectrograph and an optical intermediate-resolution spectrograph.

Finally, we examined the selection of the best quasar/LOS combination on which to perform our proposed experiment from the expected 200 SDSS quasars at $z \simeq 5$. The He I forest at $z = 5$ falls in the u' filter; consequently u' imaging is an efficient way to select the best quasar/LOS combination. However, the SDSS u' photometry will not be deep enough to detect $z \simeq 5$ quasars (any detection would be beyond the optimistic expectation of our IGM model), so follow-up u' photometry of the 200 $z \simeq 5$ quasars will be required; these observations will be inexpensive. We also consider the possibility that a quasar/LOS combination will be so good for our purposes that it falls outside of the SDSS quasar color selection criteria. This is very unlikely for quasars with ~ 10 per cent or lower transmission, but about half of all quasars with 20 per cent transmission, should any exist, would be brighter in g' than the SDSS quasar color selection limit of 22.6. If quasars are discovered with 10 per cent transmission, it may be worthwhile to modify the SDSS quasar color selection criteria so as to discover quasars with even less IGM absorption in the He I forest.

ACKNOWLEDGMENTS

MRS thanks the TA group at Harvard CfA for warm hospitality. We gratefully acknowledge helpful conversations with Wal Sargent, Rob Simcoe, Chuck Steidel, Peng Oh and Marc Kamionkowski. This work was supported in part by NASA GSRP grant NGT5-50339 and NASA grant NAG5-9821 (for MRS), and by NASA grant ATP02-0004-0093 and NSF grants AST-0071019 and AST-0204514 (for AL). AL acknowledges support from the Institute for Advanced Study and the John Simon Guggenheim Memorial Fellowship.

REFERENCES

- Anderson S.F., et al., 2001, AJ, 122, 503
- Barger A.J., Cowie L.L., Capak P., Alexander D.M., Bauer F.E., Brandt W.N., Garmire G.P., Hornschemeier A.E., 2003, ApJ, 584, L61
- Barkana R., Loeb A., 2001, Physics Reports, 349, 125
- Bechtold J., 1994, ApJS, 91, 1
- Bechtold J., 2003, in Pérez-Fournon I., Balcells M., Moreno-Insertis F., Sánchez F., eds, Galaxies at High Redshift. Cambridge Univ. Press, Cambridge, p. 131 (astro-ph/0112521)
- Becker R.H., et al., 2001, AJ, 122, 2850
- Bromm V., Kudritzki R.P., Loeb A., 2001, ApJ, 552, 464
- Burles S., Nollet K.M., Turner M.S., 2001, ApJ, 552, L1

- Cen R., 2003a, ApJ, submitted, astro-ph/0210473
 Cen R., 2003b, ApJ, submitted, astro-ph/0303236
 Djorgovski S.G., Castro S., Stern D., Mahabal A.A., 2001, ApJ, 560, L5
 Dobrzycki A., Bechtold J., Scott J., Morita M., 2002, ApJ, 571, 654
 Fan X., et al., 1999, AJ, 118, 1
 Fan X., et al., 2001a, AJ, 121, 31
 Fan X., et al., 2001b, AJ, 121, 54
 Fan X., et al., 2002, AJ, 123, 1247
 Haardt F., Madau P., 1996, ApJ, 461, 20
 Hewitt A., Burbidge G., 1987, ApJS, 63, 1
 Jakobsen P., Bokserberg A., Deharveng J.M., Greenfield P., Jedrzejewski R., Paresce F., 1994, Nature, 370, 35
 Jakobsen P., 1998, A&A, 335, 876
 Kim T.-S., Hu E.M., Cowie L.L., Songaila A., 1997, AJ, 114, 1
 Kriss G.A., et al., 2001, Science, 293, 1112
 Kogut A., et al., 2003, ApJ, submitted, astro-ph/0302213
 Leitherer C., et al., 1999, ApJS, 123, 3
 Liske J., Webb J.K., Williger G.M., Fernández-Soto A., Carswell R.F., 2000, MNRAS, 311, 657
 Loeb A., Barkana R., 2001, ARA&A, 39, 19
 McCarthy J.K., et al., 1998, in D'odorico S., ed, Proc. SPIE Vol. 3355, Optical Astronomical Instrumentation. p. 81
 Miralda-Escudé J., Ostriker J.P., 1992, ApJ, 392, 15
 Møller P., Jakobsen P., 1990, A&A, 228, 299
 Oh S.P., 2001, ApJ, 553, 499
 Oke J.B., et al., 1995, PASP, 107, 375
 Osterbrock D.E., 1989, Astrophysics of Gaseous Nebulae and Active Galactic Nuclei. University Science Books, Sausalito, CA
 Peebles P.J.E., 1993, Principles of Physical Cosmology. Princeton University Press, Princeton, NJ
 Prochaska, J.X., et al., 2001, ApJS, 137, 21
 Sargent W.L.W., Steidel C.C., Bokserberg A., 1989, ApJS, 69, 703
 Scheffler H., Elsässer H., 1988, Physics of the Galaxy and Interstellar Matter. Springer-Verlag, New York
 Schneider D.P., et al., 2002, AJ, 123, 567
 Scott J., Bechtold J., Morita M., Dobrzycki A., Kulkarni V.P., 2002, ApJ, 571, 665
 Sheinis A.I., Bolte M., Epps H.W., Kibrick R.I., Miller J.S., Radovan M.V., Bigelow B.C., Sutin B.M., 2002, PASP, 114, 851
 Spergel D.N., et al., 2003, ApJ, submitted, astro-ph/0302209
 Stengler-Larrea E.A., et al., 1995, ApJ, 444, 64
 Storrie-Lombardi L.J., McMahon R.G., Irwin M.J., Hazard C., 1994, ApJ, 427, L13
 Storrie-Lombardi L.J., Wolfe A.M., 2000, ApJ, 543, 552
 Telfer R.C., Zheng W., Kriss G.A., Davidsen A.F., 2002, ApJ, 565, 773
 Theuns T., Bernardi M., Frieman J., Hewett P., Schaye J., Sheth R. K., Subbarao M., 2002, ApJ, 574, L111
 Vanden Berk D.E., et al., 2001, AJ, 122, 549
 Verner D.A., Ferland G.J., Korista K.T., Yakovlev D.G., 1996, ApJ, 465, 487
 Weymann R., et al., 1998, ApJ, 506, 1
 White R.L., Becker R.H., Fan X., Strauss M.A., 2003, AJ, submitted, astro-ph/0303476
 Wyithe J.S.B., Loeb, A., 2003, ApJ, submitted, astro-ph/0302297
 Zheng W., Kriss G.A., Telfer R.C., Grimes J.P., Davidsen A.F., 1997, ApJ, 475, 469
 Zuo L., Phinney E.S., 1993, ApJ, 418, 28

This paper has been typeset from a \TeX / \LaTeX file prepared by the author.